Natural frequency of a composite girder with corrugated steel web

Jiho Moon [1a], Hee-Jung Ko [2b], Ik Hyun Sung [3c] and Hak-Eun Lee [*2]

[1] *New Transportation Research Center, Korea Railroad Research Institute* (*KRRI*),
Uiwang-si, Gyeonggi-do, Republic of Korea
[2] *School of Civil, Environmental & Architectural Engineering, Korea University, Seoul, Republic of Korea*
[3] *Department of Civil Engineering, Hanseo University, Chung Nam, Republic of Korea*

Abstract. This paper presents the natural frequency of a composite girder with corrugated steel web (CGCSW). A corrugated steel web has negligible in-plane axial stiffness, due to the unique characteristic of corrugated steel webs, which is called the accordion effect. Thus, the corrugated steel web only resists shear force. Further, the shear buckling resistance and out-of-plane stiffness of the web can be enhanced by using a corrugated steel web, since the inclined panels serve as transverse stiffeners. To take these advantages, the corrugated steel web has been used as an alternative to the conventional pre-stressed concrete girder. However, studies about the dynamic characteristics, such as the natural frequency of a CGCSW, have not been sufficiently reported, and it is expected that the natural frequency of a CGCSW is different from that of a composite girder with flat web due to the unique characteristic of the corrugated steel web. In this study, the natural frequency of a CGCSW was investigated through a series of experimental studies and finite element analysis. An experimental study was conducted to evaluate the natural frequency of CGCSW, and the results were compared with those from finite element analysis for verification purpose. A parametric study was then performed to investigate the effect of the geometric characteristics of the corrugated steel web on the natural frequency of the CGCSW. Finally, a simplified beam model to predict the natural frequency of a CGCSW was suggested.

Keywords: natural frequency; corrugated steel web; steel-concrete composite structures

1. Introduction

Corrugated steel plates have been used as building and bridge components due to several advantages, such as high shear buckling resistance, and out-of-plane bending stiffness (Hamilton 1993). In particular, the corrugated steel web has negligible bending capacity due to the accordion effect (Hamilton 1993, Elgaaly *et al*. 1997). As a result a corrugated steel web carries only shear forces, and the flanges and concrete slab carry the axial and bending normal stresses. Thus, the

∗Corresponding author, Professor, E-mail: helee@korea.ac.kr
[a] Senior Researcher, E-mail: jmoon1979@gmail.com
[b] Ph.D. Candidate, E-mail: atta729@naver.com
[c] Professor, E-mail: iksung@hanseo.ac.kr

efficiency of pre-stressing can be enhanced by using a corrugated steel web instead of a conventional flat web. To take advantage of these factors, the composite girder with corrugated steel web (CGCSW) has been used in France, Japan, and South Korea as an alternative to the conventional pre-stressed concrete bridge. Further, the use of the corrugated steel web provides high fatigue resistance, by minimization of the welding process, and can overcome the disadvantages of conventional stiffened flat webs such as web instability due to bending normal stress (Ibrahim *et al.* 2006, Abbas *et al.* 2007).

A typical composite girder with corrugated steel web (CGCSW) is shown in Fig. 1. An upper and lower concrete slab were connected to an I-girder with corrugated steel web with mechanical connectors such as shear studs, where the I-girder with corrugated steel web consists of two steel flanges welded to the corrugated steel web. The *x*, *y*, and *z* axes shown in Fig. 1 are the global coordinates used in this study. The corrugated steel web could have a sinusoidal or trapezoidal shape, and only trapezoidal corrugated steel webs are considered in this study. The trapezoidal corrugated steel web is composed of a series of plane and inclined sub-panels, as shown in Fig. 1, where *a* is the length of the flat panel, *c* is the length of the inclined panel, *b* is the projection length of the inclined panel, θ is the corrugation angle, t_w is the thickness of the corrugated webs, and *d* is the maximum depth of corrugation.

Research on the corrugated steel web was initiated by Easley and McFarland (1969). Since then, numerous theoretical and experimental researches on the static and buckling behavior of the behavior of corrugated steel webs have been studied (Yoda *et al.* 1994, Luo and Edlund 1996, Elgaaly *et al.* 1997, Chan *et al.* 2002, Ibrahim *et al.* 2006, Abbas *et al.* 2007, Yi *et al.* 2008, Biancolini *et al.* 2009, Kiymaz *et al.* 2010, Moon *et al.* 2009a, b, 2013, Ko *et al.* 2013, Ding *et al.* 2013). However, studies about dynamic characteristics, such as the natural frequency of a CGCSW, have rarely been reported, even if the natural frequency is essential information for dynamic analysis. It is also expected that the natural frequency of a CGCSW is different from that of a composite girder with flat web due to several unique characteristics of the corrugated steel web.
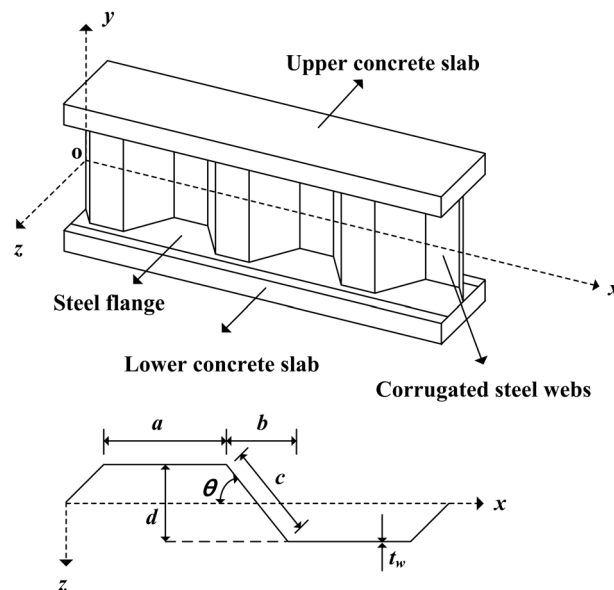

Fig. 1 Composite girder with corrugated steel web (CGCSW) and corrugation profiles

As mentioned before, the natural frequency is important for the design of the bridge, since it gives a fundamental basis for dynamic analysis, such as response spectrum analysis for the seismic design of abridge. The grid (or beam) modeling approach is often used in analysis of a bridge system, and it is doubtful that the conventional section properties of the girder with flat web are applicable to CGCSW. Thus, it is crucial to thoroughly understand the natural frequency of a CGCSW, and provide a simplified beam modeling approach with a good degree of accuracy.

In this study, the natural frequency of a CGCSW was investigated through a series of experimental programs and finite element analysis. A large scale specimen of CGCSW was constructed and tested to evaluate the natural frequency of the CGCSW. The test results were then compared with 3D finite element analysis results for verification purpose. Based on the verified finite element model, a series of parametric studies was then conducted to investigate the effect of geometrical characteristics of the corrugated steel web on the natural frequency. Finally, a simplified beam modeling approach to evaluate the natural frequency of a CGCSW was suggested for practical design purpose. It was found that the proposed model gave reasonable prediction of the natural frequency of a CGCSW without significant loss of accuracy for a practical range of corrugation profiles.

2. Experimental study

2.1 Description of experimental program

A large scale test specimen of composite girder with corrugated steel web (CGCSW) was constructed. Fig. 2(a) shows the dimensions of the test specimen. The span length of the specimen was 10.3 m. The width of the flat panel a was 180 mm, the projection width of the inclined panel b was 140 mm, the maximum depth of corrugation d was 100 mm, the thickness of the corrugated steel web t_w was 8 mm, and the height of the corrugated steel web h_w was taken as 1000 mm. As a result, a/h_w was 0.18, θ was 35.5°, and the length reduction factor η, which is defined as $(a+b)/(a+c)$, was 0.91. These values were selected to have similar corrugation profiles to existing CGCSW bridges. For existing bridges with corrugated steel webs, typical ranges of corrugation profiles are as follows: (1) $0.11 \leq a/h_w \leq 0.21$, (2) $25° \leq \theta \leq 37°$, and (3) $0.9 \leq \eta \leq 0.95$. (Moon *et al*. 2009b). The steel flange was attached to the top and bottom of the corrugated steel web, and connected to the upper and lower concrete slab with shear studs to ensure composite action of the CGCSW. The diameter of the shear stud was 19 mm. The shear studs spaced at 150 mm in the longitudinal direction of the steel flange, and 3 shear studs were installed in the transverse direction of the steel flange. The width and thickness of the top and bottom steel flange were 300 mm and 15 mm, respectively. The width and height of the upper and lower concrete slab were 500 mm and 250 mm, respectively. Four bracings were installed, to guarantee the safety for unexpected overturning of the test specimen, as shown in Fig. 2(a). It should be noted that these bracings were not in contact with the test specimen.

The impact hammer shown in Fig. 2(b) was used to apply an impulsive load to the test specimen, where the mass of the impact hammer was 5.5 kg. An impact was added on the center of the top concrete slab in the in-plane direction, and acceleration data was obtained with the time interval of 0.004 sec. Then, the natural frequency of the CGCSW was evaluated from Fast Fourier Transform (FFT) analysis with acceleration data obtained from free vibration test. To ensure the reoccurrence of the natural frequency, the same test was conducted more than 10 times.
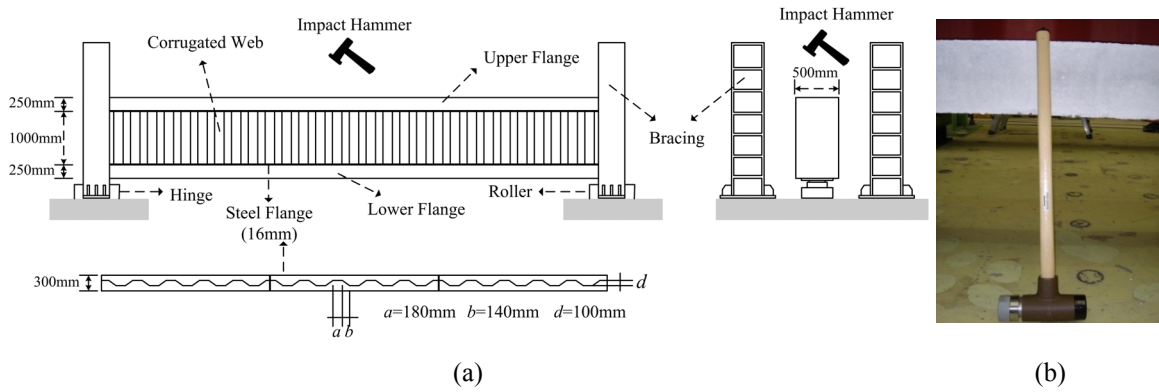
Fig. 2 Test specimen and setup: (a) dimensions of test specimen; and (b) impact hammer

Fig. 3 Details of end supports: (a) spherical bearing (hinge); and (b) spherical bearing (roller)

Fig. 3 shows the details of end supports used in the test. The test specimen was simply supported, and full scale spherical bearings were used to reflect the practical end condition of real construction. Eight servo accelerometers were used to measure the acceleration generated by impulsive load, and the arrangement of accelerometers is shown in Fig. 4, where the vibration frequency ranges of servo accelerometers used in this study varies from 1 Hz to 250 Hz.

The CGCSW is usually pre-stressed, by using internal tendons to control the cracks in a concrete slab in the service load level. Further, external tendons are sometimes used, if necessary. In this study, the effect of internal and external tendon on the natural frequency of CGCSW was investigated, through a series of experimental studies. Table 1 shows the details of test specimens. The NT specimen served as the base model, and had no internal or external tendons. E0_I1 in Table 1 had only two internal tendons in the center of the lower concrete slab, where the jacking force was 208.53 kN. The ratio of jacking force to ultimate tendon force was 0.8, and the ratio between total jacking forces and theoretical axial capacity of the specimen was approximately 6.1%. It is noted that SWPC 7B tendon was used for both internal and external tendons, where the area and ultimate tendon force of SWPC 7B are 138.7 mm^2 and 260.8 kN, respectively. In the case of test specimens with external tendons (E1_I0 - E6_I0 in Table 1), the external tendons were
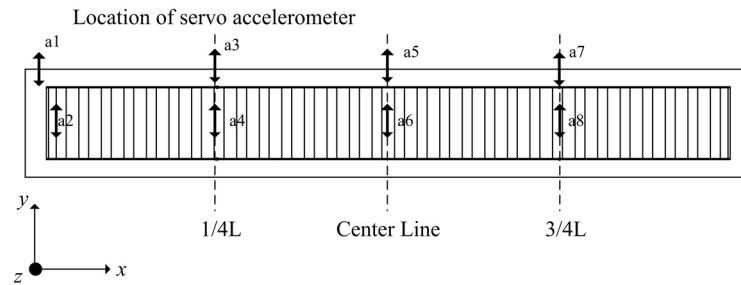
Fig. 4 Arrangement of servo accelerometers

Table 1 Details of test specimens

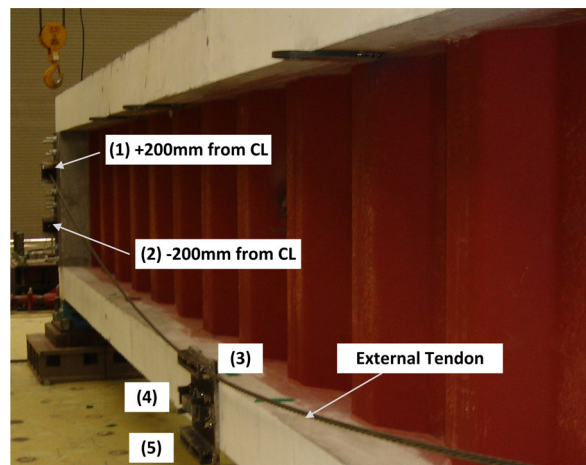| Model	Internal tendon	External tendon	Location of end anchorage	Location of center anchorage	Angle (degree)	Jacking force (kN)	Jacking force/ ultimate tendon force
NT	x	x	N/A	N/A	N/A	N/A	N/A
E1_I0	x	o	(1)	(3)	8	229.12	0.88
E2_I0	x	o	(1)	(4)	10	175.03	0.67
E3_I0	x	o	(1)	(5)	11	141.90	0.54
E4_I0	x	o	(2)	(3)	3	227.36	0.87
E5_I0	x	o	(2)	(4)	5	173.17	0.66
E6_I0	x	o	(2)	(5)	7	140.04	0.54
E0_I1	o	x	N/A	N/A	0	208.54	0.80

Fig. 5 External tendon and location of anchorages

installed on both sides of the test specimen, and the angle of external tendons varied from 3° to 11°, by changing the location of the end and center anchorages. The locations of the end and center anchorage are shown in Fig. 5. The jacking forces of E1_I0-E6_I0 were determined to induce the in-plane bending moment of 107.9 kN·m at the center of the test specimens. The ratios of jacking

force to ultimate tendon force of E1_I0 - E6_I0 varied from 0.54 to 0.88, as shown in Table 1. The ultimate flexural strength of the specimen was obtained from the test, and the ratio between in-plane bending moment due to external tendons and ultimate flexural strength of the specimen was approximately 5.5%.

2.2 Test results

Fig. 6 shows the acceleration data obtained from the free vibration test and FFT analysis for a3, a4, and a8 accelerometers of the NT specimen shown in Table 1. The FFT analysis results were almost identical to each other, regardless of the location of accelerometer, as shown in Fig. 6. All natural frequencies of NT specimen obtained from a1-a8 accelerometers are summarized in Table 2. The variation of the natural frequency was negligible. For the 1st and 2nd natural frequency shown in Table 2, the maximum difference was 0.7 and 1.7%, for the 1st and 2nd natural frequency, respectively. In this study, the natural frequency of the test specimen was evaluated based on the acceleration data of a3 accelerometer for all specimens, since the variation of the natural frequency depending on the location of accelerometer was very small. As mentioned before, the same test was conducted more than 10 times for each case to ensure the reoccurrence of the natural frequency. Thus, the natural frequency of test specimens was determined by averaging the FFT results of a3 accelerometer for each case, and the results are summarized in Table 3.

From Table 3, it was found that the 1st and 2nd average natural frequencies of test specimens were almost identical to each other regardless of the existence of internal or external tendons. The maximum discrepancy was 1% for both 1st and 2nd average natural frequency, as shown in Table 3. This is because the mass of the internal and external tendon was very small compared with that of the test specimens. Further, the applied moment and axial force induced by internal or external tendons were also small compared with the bending and axial load capacity of the specimen without internal or external tendon. Thus, effect of internal and external tendons on the natural frequency was insignificant.
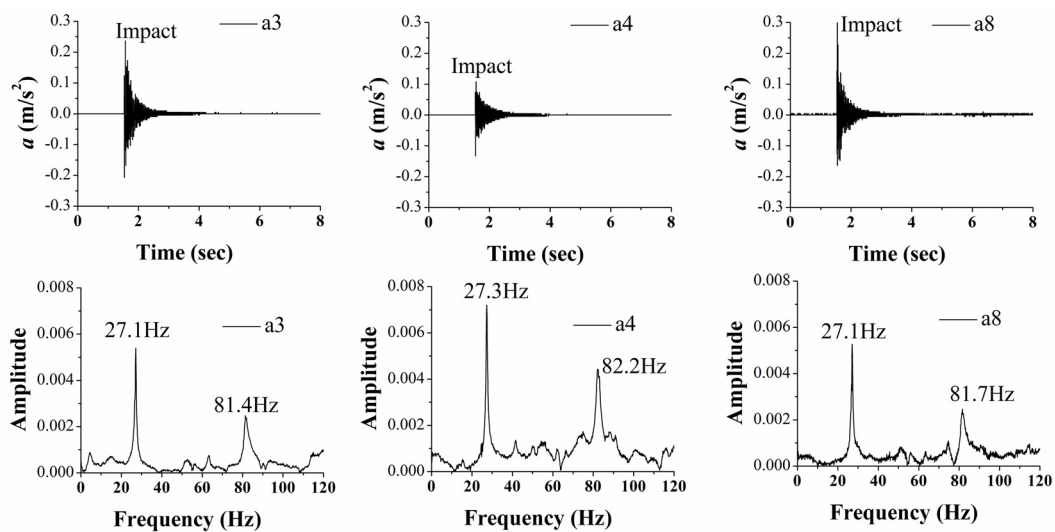

Fig. 6 Acceleration data vs. time and FFT analysis results for a3, a4 and a8 accelerometers (NT specimen)

Table 2 Summary of the 1st and 2nd natural frequency (NT specimen)

	a1	a2	a3	a4	a5	a6	a7	a8	Max. difference (%)
1st natural frequency (Hz)	27.2	27.3	27.1	27.3	27.2	N/A	27.1	27.1	0.7
2nd natural frequency (Hz)	82.6	82.8	81.4	82.2	82.2	N/A	81.7	81.7	1.7

Table 3 Summary of average natural frequency of test specimens

Model	1staverage natural frequency (Hz)	2ndaverage natural frequency (Hz)
NT	27.1	81.4
E1I0	27.3	82.2
E2I0	27.2	82.4
E3I0	27.2	81.5
E4I0	27.3	82.4
E5I0	27.2	82.4
E6I0	27.2	82.2
E0I1	27.1	81.8

It is expected that the 1st and 2nd average natural frequencies shown in Table 3 may be the 1st and 2nd in-plane bending natural frequencies, since the impact was applied at the center of the upper concrete slab in the in-plane direction. However, it is hard to visualize the deformation shape based on the acceleration data. Thus, three-dimensional finite element analysis was conducted to identify the deformation shape of the test specimen, and to verify the finite element model, as well.

3. Finite element modeling and verification

Finite element analysis was performed by using a general purpose structural analysis program ABAQUS (2009). Fig. 7 represents the finite element model used to simulate the NT specimen. An 8-node solid element, 4-node shell element, and 2-node truss element were used to model the concrete slab, steel sections, and reinforcing bar, respectively. The reinforcing bar was embedded into the concrete slab by using the EMBEDED option in ABAUQS (2009), and it is assumed that the reinforcing bar and concrete were perfectly bonded. The concrete slabs and steel flanges were also perfectly bonded by using the TIE option in ABAQUS (2009), since the concrete slabs and steel flanges were connected by shear studs, and the slip is negligible for small loading, such as the impulsive loading induced by impact hammer used in this study for the free vibration test. The stress-strain relationship of materials was assumed as linear elastic. The elastic modulus of concrete and steel were taken as 28,000 MPa and 210,000 MPa, respectively. The mass density of the concrete and steel were assumed as 2,500 kg/m^3 and 7,850 kg/m^3, respectively. The boundary condition is also shown in Fig. 7. For hinge support, displacements in the x, y, and z directions were restrained, while displacement in the y and z axes were constrained for roller support.
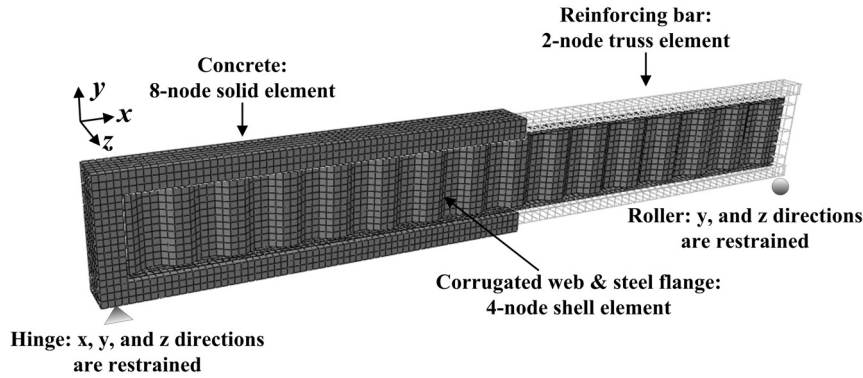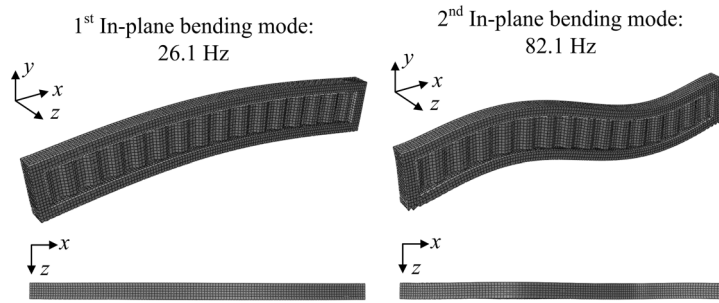
Fig. 7 Finite element model of NT specimen

Fig. 8 Natural frequencies and mode shapes for 1st and 2nd in-plane bending

Table 4 Summary of analysis results (NT specimen)

	1st	2nd	3rd	4th	5th	6th	7th	9th	9th	10th
Frequency (Hz)	8.4	19.6	25.1	26.1	40.1	43.1	54.2	64.5	71.9	82.1
Mode	OB & T	OB & T	OB & T	IB	OB & T	OB & T	A & IB	OB & T	OB & T	IB

*Note: A, IB, OB, and T represent axial, in-plane bending, out-of-plane bending, and torsional mode, respectively

Fig. 8 shows the natural frequencies and corresponding mode shapes obtained from finite element analysis for 1st and 2nd in-plane bending. Table 4 shows a summary of the analysis results for the NT specimen. From the analysis results, in-plane bending mode shapes were observed at the 4th and 10th mode shape, as shown in Table 4. For these mode shapes, the analysis model deflects in the in-plane direction with negligible out-of-plane displacement, as shown in Fig. 8. The 1st and 2nd in-plane bending natural frequencies were 26.1 and 82.1 Hz, respectively. Compared with the test results of the NT specimen, the difference between test and analysis was 4% and 1% for the 1st and 2nd mode, respectively. Thus, it can be concluded that the 1st and 2nd average natural frequency obtained from the test represents the 1st and 2nd in-plane bending mode shapes, respectively. Further, it can be found that the 3D finite element model used in this study

provided good prediction of the natural frequency of the CGCSW.

4. Parametric study

A series of parametric studies was conducted to investigate the effect of the geometric characteristics of the corrugated steel web on the natural frequency of the CGCSW by using the verified 3D finite element model. Table 5 shows the profiles of the analysis model for the parametric study. The analysis model was selected similar to the test specimen. The length of the model was 10 m, width of the concrete slab b was 500 mm, and the thickness of the concrete slab t was 250 mm. The width and thickness of steel flange (b_f and t_f) were 250 mm and 15 mm, respectively. For the corrugated steel webs, the width of flat panel a, and the projection length of inclined panel b were 180 mm and 140 mm, respectively. The maximum corrugation depth d is the main parameter, and d varied from 25 to 120. As a result, the corrugation angle θ ranged from 10.1° to 40.6°. Stirrups were installed in the upper and lower concrete slabs with a spacing of 125 mm, where D10 bar was used (the area of D10 bar is 71.33 mm^2). Four longitudinal reinforcing bars were also installed in the concrete slabs, where D17 bar was used (the area of D17 is 198.6 mm^2). The resulting longitudinal reinforcement ratio was 0.64 %.

Hinge and roller supports were assumed at the center of the left and right ends of the analysis model, as shown in Fig. 9. Displacements in the x, y, and z direction were restrained for the hinge support, while displacements in the y and z axes were constrained for roller support. In addition, rotation about the x axis was constrained for both hinge and roller. Finally, displacements in the y, and z directions of the right and left ends were restrained to prevent distortion of the cross section.

The results of parametric study are shown in Fig. 10. In Fig. 10, x and y axes represent the corrugation angle and normalized natural frequency, respectively. It is noted that the natural
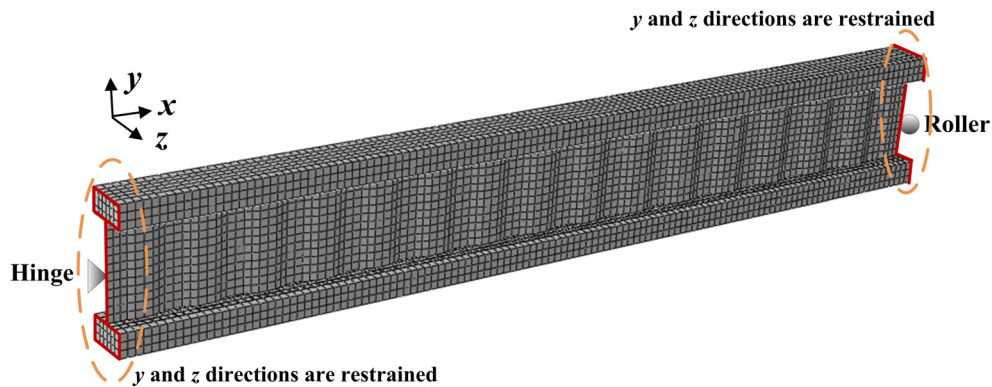

Fig. 9 Finite element model and boundary condition for parametric study

Table 5 Profiles of the finite element models for parametric study

L (mm)	b (mm)	t (mm)	b_f (mm)	t_f (mm)	h_w (mm)	t_w (mm)	a (mm)	b (mm)	d (mm)	θ (°)
10,000	500	250	250	15	1000	8	180	140	25-120	10.1-40.6

frequency was normalized with the results of the analysis model with $\theta = 10.1°$ (the smallest θ among the analysis models). From Fig. 10 (a), it can be seen that the in-plane natural frequency of CGCSW slightly decreased with increasing corrugation angle θ. The natural frequency was approximately 2.5% decreased with increasing θ from 10.1° to 40.6°. This is because the in-plane bending stiffness of CGCSW remains constant, while the total mass of CGCSW slightly increases with increasing θ. The effect of the corrugated steel web on the in-plane bending stiffness is usually ignored, because it is assumed that the corrugated steel web has negligible axial stiffness due to the accordion effect. Thus, the bending stiffness is all the same for the analysis models, while the total mass of the CGCSW slightly increases with increasing θ, since the unfolded length of the corrugated steel web increases with increasing θ. For example, the total mass of CGCSW increases 1.1% with increasing θ from 10.1° to 40.6° for the analysis models used in this study.

Fig. 11 shows the 1st and 2nd in-plane bending modes of the analysis model with $\theta = 10.1°$ and 40.6°. It can be seen that the 1st in-plane bending mode of the model having θ of 10.1° is similar with the model having θ of 40.6°. Also, negligible out-of-plane displacements of the concrete slabs were observed for both models. However, for the 2nd in-plane bending mode, the out-of-plane
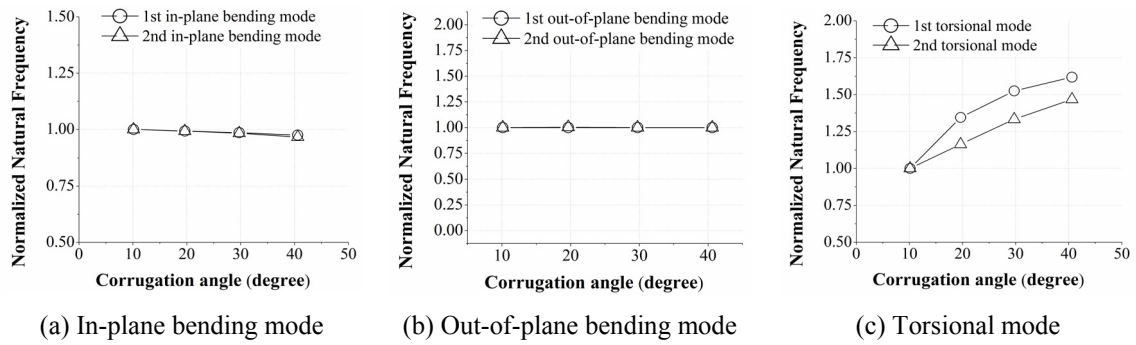

(a) In-plane bending mode   (b) Out-of-plane bending mode   (c) Torsional mode
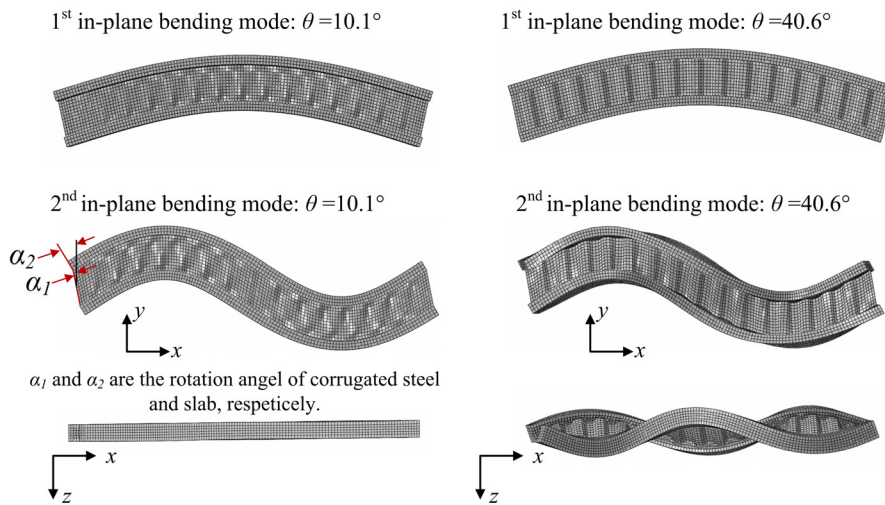
Fig. 10 Natural frequency vs. corrugation angle

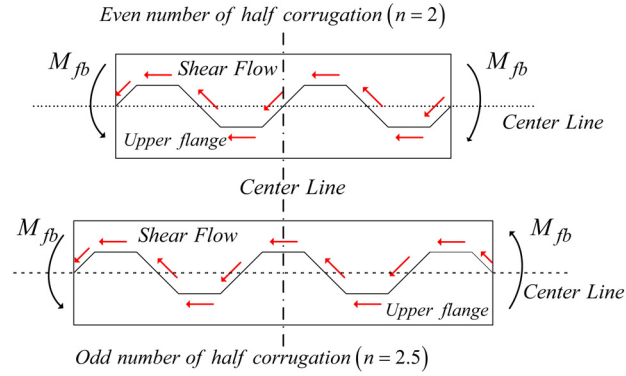Fig. 11 In-plane bending mode of analysis models (θ=10.1, and 40.6°)

Fig. 12 Flange bending mechanism of I-girder with corrugated webs

displacements of the concrete slabs of the analysis model with $\theta = 40.6°$ werevery large, as shown in Fig. 11. These out-of-plane displacements are generated by the shear flow acting along the edge of the corrugated steel web. Fig. 12 shows the flange bending moment mechanism of an I-girder with corrugated steel web (Abbas *et al*. 2007, and Moon *et al*. 2013). The shear flow acting along the corrugated steel web generates flange bending moment M_f, as shown in Fig. 12, and the magnitude of M_f increases with increasing corrugation depth d(or corrugation angle θ).Thus, for the analysis model with $\theta = 40.6°$, the in-plane bending mode was combined with the torsional mode. It was also found that the rotational angle of the corrugated steel web (α_1 in Fig. 11) was considerably different from that of the concrete slab (α_2 in Fig. 11). These results imply that shear deformation of the corrugated steel web affectsα_1. Machindamrong *et al*. (2004) indicated that the effect of shear deformation of the corrugated steel web on the in-plane deflection is considerable. A similar result was observed from the deformation shape of the in-plane bending mode shown in Fig. 11, and the effect of shear deformation was more significant for the 2nd in-plane bending mode comparing with the 1st mode.
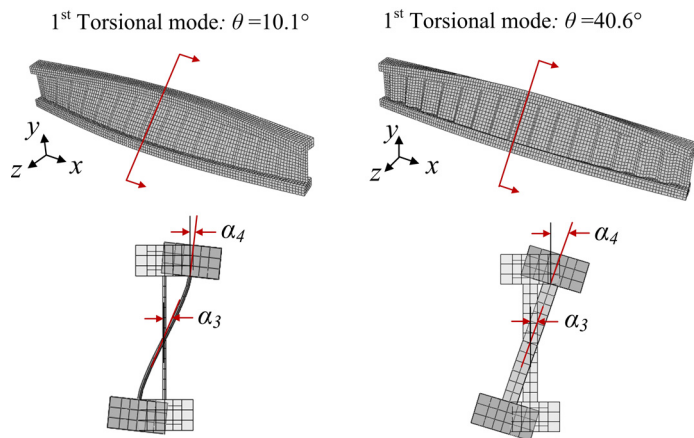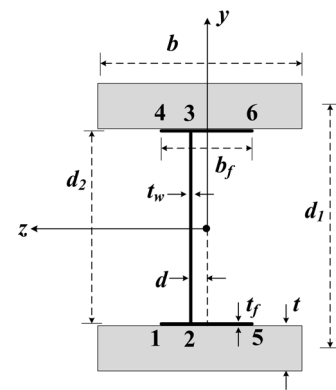

Fig. 13 Torsional mode of analysis models ($\theta = 10.1$, and 40.6°)

Fig. 14 Dimensions of CGCSW

In the case of the out-of-plane bending natural frequency of CGCSW, the natural frequency is almost identical, regardless of θ, as shown in Fig. 10(b). This is because the out-of-plane stiffness of the corrugated steel web and total mass of the CGCSW slightly increase at the same time with increasing θ (or corrugation depth d). The corrugated steel web is eccentrically attached with the maximum corrugation depth d to the steel flanges and concrete slabs (refer Fig. 1). The out-of-plane bending stiffness of the corrugated steel web about the center of the steel flanges and concrete slabs is equal to $(h_w t_w^3)/12 + (h_w t_w) d_{avg}^2/4$, where d_{avg} is the average corrugation depth (the details of the out-of-plane bending stiffness of the CGCSW are shown in Section 5). Thus, the out-of-plane bending stiffness increases with increasing d. For example, the out-of-plane bending stiffness of the analysis models increases approximately 2.2% with increasing θ from 10.1° to 40.6°.

Fig. 10(c) shows the variation of the torsional natural frequency of the CGCSW in θ. The torsional natural frequency increases significantly with increasing θ. Fig. 13 represents the torsional mode of the analysis models with $\theta = 10.1°$ and 40.6°. For the analysis model with $\theta = 10.1°$, the twisting angle of the corrugated steel web (α_3 in Fig. 13) was larger than the twisting angle of the concrete slab (α_4 in Fig. 13). This implies that the concrete slabs were not fully twisted, since the bending stiffness of the corrugated steel web itself about the x axis is too small to transfer the full twisting moment to the concrete slabs. The bending stiffness of the corrugated steel web about the x axis is a function of the corrugation depth d, and the stiffness increases with increasing d (or θ). For the model with $\theta = 40.6°$, the torsional angle of the corrugated steel web and the concrete slab was almost identical each other. As a results, the torsional natural frequency of the CGCSW increases with increasing θ.

5. Simplified beam model approach to predict the natural frequency of CGCSW

The effect of corrugation profiles on the natural frequency was investigated by using 3D finite element analysis in the previous section. 3D finite element analysis provides accurate estimation of the natural frequency, and corresponding mode shape of the CGCSW. However, 3D finite element analysis is not suitable for design purposes, since sometimes designers have to model the entire structural system, and 3D finite element analysis is a somewhat time consuming procedure for this. Thus, it is logical to develop a simplified beam model approach to predict the natural frequency of the CGCSW. To apply a simplified beam model approach to evaluate the natural frequency of the CGCSW, the static sectional properties of the CGCSW must be evaluated first, and the section properties of the CGCSW were proposed herein.

As mentioned before, the corrugated steel web has negligible axial stiffness. Thus, ignoring the effect of the corrugated steel web on the bending stiffness about the z axis (in-plane bending or bending stiffness about the strong axis), the effective bending stiffness about the z axis can be expressed as

$$EI_{eff.z} = E_c \left(\frac{bt^3}{6} + \frac{btd_1^2}{2} \right) + E_s \left(\frac{b_f t_f^3}{6} + \frac{b_f t_f d_2^2}{2} \right) \tag{1}$$

where, d_1 is the distance from the center of the lower steel flange to the center of the upper steel flange, and d_2 is the distance from the center of the lower concrete slab to the center of the upper concrete slab (refer Fig. 14). E_c and E_s are the modulus of elasticity of the concrete and steel, respectively.

The effective bending stiffness of CGCSW about the y axis (Weak axis) is also obtained as

$$EI_{eff,y} = E_c\left(\frac{tb^3}{6}\right) + E_s\left(\frac{t_f b_f^3}{6}\right) + E_s\left(\frac{h_w t_w^3}{12} + h_w t_w d_{avg}^2\right) \tag{2}$$

It is noted that the first and second term in Eq. (2) are the bending stiffness about the y axis of the concrete slab and the steel flange, respectively. The third term in Eq. (2) represents the effect of the corrugated steel web on the bending stiffness about the y axis. The corrugated steel web is eccentrically attached to the steel flanges, and the depth varies along the length of the girder. Thus, in this study, the average corrugation depth d_{avg} was used (Moon *et al.* 2009a). The average corrugation depth can be expressed as

$$d_{avg} = \frac{(2a+b)d}{4(a+b)} \tag{3}$$

The effective pure torsional rigidity of the CGCSW can be calculated as the sum of the pure torsional rigidity of the concrete slabs and the steel section. The pure torsional rigidity of the steel section is equal to the sum of the pure torsional constants of each individual steel plate element. In the case of the concrete slabs, an approximated solution for the pure torsional constant J of rectangular section can be used. For a rectangular section, J can be expressed as a function of the area A and the polar moment of inertia I_r of the rectangular section, and it is given by (Heins 1975)

$$J = \frac{A^4}{40 I_r} \tag{4}$$

Thus, the effective pure torsional rigidity of the CGCSW is calculated as

$$GJ_{eff} = G_c\left(\frac{3}{5}\frac{b^3 t^3}{(b^2+t^2)}\right) + G_{s,co}\left(\frac{2}{3}b_f t_f^3 + \frac{h_w t_w^3}{3}\right) \tag{5}$$

where, $G_{s,co}$ is the shear modulus of the corrugated steel plate. Generally, the shear modulus of a corrugated plate is smaller than that of a flat plate. The shear modulus of the corrugated steel plate used in this study is proposed by Samanta and Mukhopadhyay (1999). The shear modulus $G_{s,co}$ of the corrugated plate is defined as

$$G_{s,co} = \frac{(a+b)}{(a+c)}G = \eta G \tag{6}$$

In Eq. (6), G is the shear modulus of the flat plate, and η is the ratio of the actual length of the corrugated plate $(a + c)$ to its projected length $(a + b)$.

CGCSW is basically an open section. Thus, the warping constant of the CGCSW should be evaluated. Moon *et al.* (2009a) theoretically derived the warping constant of the I-girder with corrugated steel web, and their equation was adopted to evaluate the warping constant of the steel section. The warping constant of the I-girder with corrugated steel web $C_{w,co}$ is given by

$$C_{w,co} = \frac{1}{3}\sum\left(W_{ni}^2 + W_{nj}W_{ni} + W_{nj}^2\right)t_{ij}l_{ij} \tag{7}$$

in which

$$W_{n1} = \frac{2b_f^2 h_w t_f}{8b_f t_f + 4h_w t_w}, \qquad\qquad W_{n2} = \frac{2b_f^2 h_w t_f + b_f h_w^2 t_w}{8b_f t_f + 4h_w t_w} - \left(\frac{b_f}{4} - \frac{d_{avg}}{2}\right) h_w$$

$$W_{n3} = \frac{2b_f^2 h_w t_f + b_f h_w^2 t_w}{8b_f t_f + 4h_w t_w} - \left(\frac{b_f}{4} + \frac{d_{avg}}{2}\right) h_w, \quad W_{n4} = \frac{2b_f^2 h_w t_f + b_f h_w^2 t_w}{8b_f t_f + 4h_w t_w} - \frac{1}{2}b_f h_w,$$

$$W_{n5} = W_{n4} \quad \text{and} \quad W_{n6} = W_{n1}$$

(8)

In Eq. (8), W_{ni} is the normalized unit warping at point i (location of i (1-6) is shown in Fig. 14) of any element $(i - j)$, l_{ij} is the length of plate element, t_{ij} is the thickness of plate element, and d_{avg} is the average corrugation depth. Thus, $C_{w,co}$ can be calculated as follows: (a) calculation of the d_{avg} using Eq. (3); (b) evaluation of W_{ni} using Eq. (8) with d_{avg} obtained in step (a); and (c) determination of $C_{w,co}$ using Eq. (9) with W_{ni} obtained in step (b). Finally, the effective warping rigidity of the CGCSW can be calculated by the sum of the warping rigidity of concrete and the steel part, and it is given by

$$EC_{w,eff} = E_c \left(\frac{tb^3 d_2^2}{24}\right) + E_s C_{w,co}$$

(9)

The effective axial stiffness of the CGCSW is simply obtained by ignoring the corrugated steel web, and it is given by

$$EA_{eff} = E_c(2bt) + E_s(2b_f t_f)$$

(10)

The unit density is an important parameter for the prediction of natural frequency, and the effective unit density of CGCSW can be obtained by considering the actual length of the corrugated steel web as following

$$\rho_{eff} = \frac{(2bt\rho_c + 2b_f t_f \rho_s / \eta)}{(2bt + 2b_f t_f + h_w t_w)}$$

(11)

Based on the proposed section properties and the effective unit density of the CGCSW (Eqs. (1)-(11)), the natural frequency of the analysis model shown in the previous section was re-evaluated for verification purpose. The analysis results are shown in Fig. 15.

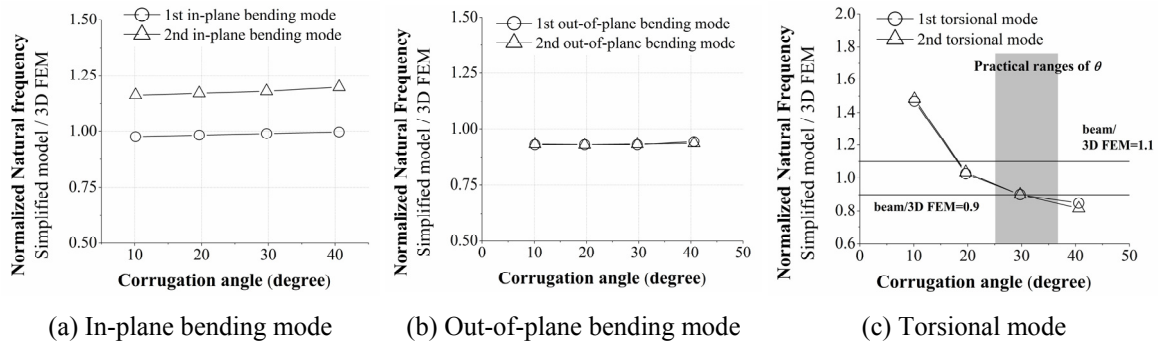(a) In-plane bending mode   (b) Out-of-plane bending mode   (c) Torsional mode

Fig. 15 Comparison of results of simplified model with those from 3D FEM

From Fig. 15, it can be found that the simplified beam model approach provided good estimation of the 1st in-plane bending mode while it over estimated the 2nd in-plane bending mode by approximately 17%. In the case of the out-of-plane bending mode, the simplified beam mode approach agreed well with the results of the 3D finite element analysis results for both 1st and 2nd modes. For the torsional mode, the beam model approach gave a very conservative prediction of the natural frequency when $\theta = 10.1°$. The twisting angle of the corrugated steel web and concrete slabs were different from each other when $\theta = 10.1°$ from the 3D finite element analysis results, since the bending stiffness of the corrugated steel web about the *x* axis is not sufficient (refer Fig. 13). However, the twisting angle of the section is uniform throughout the section for the beam model. Thus, the discrepancy is comparative large for the analysis model with small corrugation angle, such as $\theta = 10.1°$. The typical range of θ of existing bridges with corrugated steel webs varies from 25° to 37°, and the simplified beam model approach provided a reasonable estimation of the torsional natural frequency of the CGCSW with this practical range of θ, as shown in Fig. 15(c).

6. Conclusions

This study investigated the natural frequency of a composite girder with corrugated steel web (CGCSW), through a series of tests and finite element analyses. A large scale test specimen was constructed and tested to evaluate the natural frequency of the CGCSW. The major parameter of the test was the effect of internal and external tendons on the natural frequency of the CGCSW. From the test results, it was found that neither the internal nor external tendon shad significant effects on the natural frequency of the CGCSW. 3D finite element analysis was conducted for the test specimen to identify the model shape and to verify the finite element model. The finite element model was successfully verified, and a parametric study was conducted to evaluate the effect of corrugation profiles on the natural frequency of the CGCSW. From the analysis results, the following conclusions were made:

(1) The in-plane bending natural frequency slightly decreases with increasing corrugation angle, since the total mass of the CGCSW slightly increases, while the in-plane bending stiffness remains constant due to the accordion effect. Also, it was found that the in-plane bending mode was combined with the torsional mode when the corrugation angle is large, since the flange bending moment is considerable.

(2) The variation of out-of-plane bending natural frequency with the corrugation angle is negligible. This is because the total mass and out-of-plane bending stiffness of the CGCSW simultaneously increase with increasing the corrugation angle.

(3) The twisting angle of the concrete slabs and corrugated steel web were considerably different when the corrugation angle was small, since the bending stiffness of the corrugated steel web about *x* axis (Refer Fig. 12) is not sufficient. Therefore, the torsional natural frequency decreases with decreasing corrugation angle. Further, adequate corrugation depth should be provided to develop a uniform twisting angle throughout the section.

Finally, a simplified beam model approach was proposed for practical design purposes. For this, static sectional properties and the effective unit density of the CGCSW were proposed. From the comparison results with 3D finite element analysis, the proposed beam model approach provided reasonable estimation of the natural frequency of the CGCSW in a typical range of corrugation

profiles.

Acknowledgments

This research was supported by a grant from R&D Program of the Korea Railroad Research Institute, Republic of Korea. Also, it is partially supported by a Korea University Grant.

References

ABAQUS (2009), ABAQUS analysis user's manual version 6.9-2, Dassault systemes Simulia Corp. Providence, RI, USA.

Abbas, H.H., Sause, R. and Driver, R.G. (2007), "Analysis of flange transverse bending of corrugated web I-girders under in-plane loads", *J. Struct. Eng. ASCE*, **133**(3), 347-355.

Biancolini, M.E., Brutti, C. and Porziani, S. (2009), "Analysis of corrugated board panels under compression load", *Steel. Compos. Struct., Int. J.*, **9**(1), 1-17.

Chan, C.L., Khalid, Y.A., Sahari, B.B. and and Hamouda, A.M.S. (2002), "Finite element analysis of corrugated web beams under bending", *J. Constr. Steel. Res.*, **58**(11), 1391-1406.

Ding, Y., Jiang, K., Shao, F. and Deng, A. (2013), "Experimental study on ultimate torsional strength of PC composite box-girder with corrugated steel webs under pure torsion", *Struct. Eng. Mech., Int. J.*, **46**(4), 519-531.

Easley, J.T. and McFarland, D.E. (1969), "Buckling of light-gauge corrugated metal shear diaphragms", *J. Sruct. Div. ASCE*, **95**(ST7), 1497-1516.

Elgaaly, M., Seshadri, A. and Hamilton, R.W. (1997), "Bending strength of steel beams with corrugated webs", *J. Struct. Eng. ASCE*, **123**(6), 772-782.

Hamilton, R.W. (1993), "Behavior of welded girder with corrugated webs", Ph. D. Thesis, University of Maine, Orono, ME, USA.

Heins, C.P. (1975), *Bending and Torsional Design in Structural Members*, Lexington Books, MA, USA.

Ibrahim, S.A., El-Dakhakhni, W.W. and Elgaaly, M. (2006), "Behavior of bridge girder with corrugated webs under monotonic and cyclic loading", *Eng. Struct.*, **28**(14), 1941-1955.

Kiymaz, G., Coskun, E., Cosgun, C. and Seckin E. (2010), "Transverse load carrying capacity of sinusoidally corrugated steel web beams with web openings", *Steel Compos. Struct., Int. J.*, **10**(1), 69-85.

Ko, H.-J., Moon, J., Shin,Y.-W. and Lee, H.-E. (2013), "Non-linear analyses model for composite box-girders with corrugated steel webs under torsion", *Steel Compos. Struct., Int. J.*, **14**(5), 409-429.

Luo, R. and Edlund, B. (1996), "Shear capacity of plate girders with trapezoidally corrugated webs", *Thin-Wall. Struct.*, **26**(1), 19-44.

Machimdarong, C., Watanabe, E. and Utsunomiya, T. (2004), "Analysis of corrugated steel web girders by an efficient beam bending theory", *Struct. Eng. / Earthq. Eng. JSCE*, **21**(2), 131s-142s.

Moon, J., Yi, J., Choi, B.H. and Lee, H.-E. (2009a), "Lateral-torsional buckling of I-girder with corrugated webs under uniform bending", *Thin-Wall. Struct.*, **47**(1), 21-30.

Moon, J., Yi, J., Choi, B.H. and Lee, H.-E. (2009b), "Shear strength and design of trapezoidally corrugated steel webs", *J. Constr. Steel. Res.*, **65**(5), 1198-1205.

Moon, J., Lim, N.-M. and Lee, H.-E. (2013), "Moment gradient correction factor and inelastic flexural-torsional buckling of I-girder with corrugated steel webs", *Thin-Wall. Struct.*, **62**, 18-27.

Samanta, A. and Mukhopadhyay, M. (1999), "Finite element static and dynamic analyses of folded plates", *Eng. Struct.*, **21**(3), 227-287.

Yi, J., Gil, H., Youm, K. and Lee, H.-E. (2008), "Interactive shear buckling of trapezoidally corrugated webs", *Eng. Struct.*, **30**(6), 1659-1666.

Yoda, T., Ohura, T. and Sekii, K. (1994), "Analysis of composite PC Box girders with corrugated steel

webs", *Proceedings of the 4th International Conference on Short and Medium Span Bridges*, Halifax, Canada, August, pp. 1107-1115.

CC